Presented to 9th International Conference on Heavy Ion Accelerator Technology, January 14-18, 2002, New Delhi

Beam Dynamics Studies in the Driver Linac Prestripper Section of the RIA Facility[1]

E. S. Lessner and P. N. Ostroumov,

Argonne National Laboratory, 9700 S. Cass Avenue, Argonne, IL, 60439

The RIA facility driver linac consists of about 400 superconducting (SC) independently phased rf cavities. The linac is designed to accelerate simultaneously several-charge-state beams to generate as much as 400 kW of uranium beam power. The linac beam dynamics is most sensitive to the focusing and accelerating-structure parameters of the prestripper section, where the uranium beam is accelerated from 0.17 keV/u to 9.4 MeV/u. This section is designed to accept and accelerate 2 charge states (28 and 29) of uranium beam from an ECR ion source. The prestripper section must be designed to minimize the beam emittance distortion of this two-charge-state beam. In particular, the inter-cryostat spaces must be minimized and beam parameters near transitions of the accelerating and focusing lattices must be matched carefully. Several sources of possible effective emittance growth are considered in the design of the prestripper section and a tolerance budget is established. Numerical beam dynamics studies include realistic electric and magnetic 3-dimensional field distributions in the SC rf cavities and SC solenoids. Error effects in the longitudinal beam parameters are studied.

1 Introduction

The RIA Driver Linac will accelerate multiple-charge-states (multi-q) of the heaviest ion beams, for which the beam current is limited by ion-source performance. Multi-q operation can provide not only a substantial increase in beam current, but also enables the use of two strippers, reducing the size and cost of the driver linac. It should be noted, however, that multi-q operation places stringent requirements on the linac design [1]. As it was mentioned in ref. [2], a multi-q uranium beam will have larger longitudinal emittance than a single-charge-state beam. The longitudinal emittance can grow under phase and amplitude fluctuations of the accelerating field. Transverse emittance growth can occur if the focusing and accelerating elements are misaligned. To insure that all requirements can be met, the dynamics of multi-q uranium beams, from the ion source, through the driver linac, to the production targets, must be carefully studied and optimised. In particular, the prestripper section must be designed for acceleration of two-charge state beams with the lowest possible emittance growth. The main source of longitudinal effective emittance growth is non-linear particle motions in the longitudinal phase space. In a low-energy SRF linac the non-linearity of charged particle motions is caused mainly by the long drift spaces between the cavities. These drift spaces are required for placement of focusing elements.

A detailed design has been developed for the injector section of the driver linac which can provide two charge states directly from the ECR source, effectively doubling the beam current available for uranium. The acceleration of two-charge-state uranium beams is implemented in a system containing a multi-harmonic buncher and a 57.5 MHz RFQ [3].

The prestripper section of the RIA driver linac accelerates uranium ions from 170 keV/u to 9.4 MeV/u. This section can be retuned to accelerate lighter ions, in order to obtain higher beam energies per nucleon. For example, protons can be accelerated up to 45.8 MeV. The accelerating and focusing lattices of the prestripper section need to be designed to minimize appreciable emittance growth. A comprehensive study of partial effects of accelerating field random errors on the longitudinal beam parameters has been performed and it is described in this paper.

The beam dynamics design and optimisation of the prestripper linac were performed using the code TRACK [4], which integrates the charged particle motion in presence of the full six dimensional electromagnetic field. Multi-particle motion in the six-dimensional (6D) phase space is simulated by an iterative solution of the equation of motion. The code uses 48 mesh elements per accelerating cell with the length $\beta_G\lambda/2$, 8 mesh elements in the radial direction and 16 azimuthal mesh elements. Here, β_G is the geometrical beta of the cavity. The electromagnetic fields in all the prestripper linac SRF cavities were obtained with the code CST Microwave Studio (MWS) [5]. The MWS code can calculate all six components of electromagnetic field distribution within the beam-cavity interaction area with a mesh size of about 1 mm.

[1] Work supported by the U. S. Department of Energy under contract W-31-109-ENG-38.

The code 'elegant' was used as an independent evaluation of the prestripper linac beam dynamics simulations. 'elegant' was originally written to simulate electrons and was modified for simulation of two-charge state ion beams [6]. 'elegant' is a 6D accelerator program for transport lines and circular machines. The program is particularly suitable for simulations of random errors, since it allows the addition of random errors to almost any parameter of any accelerator element. Post-processing analysis and statistics are conveniently done by the SDDS Toollkit [7]. In order to emulate heavy ion dynamics, the electromagnetic fields and magnet component strengths are mapped such that:

$$E_e / (q_{HI} E_{HI}) = - m_e / (A_{HI} \text{ a.m.u.}),$$

where E_e and E_{HI} stand for the electron- and ion- field strengths, respectively; m_e is the electron mass, and A_{HI} is the ion atomic number.

Since space charge effects are negligible in the prestripper linac, simulation of a two-charge-state beam can be done sequentially, each equivalent electron bunch accelerated by fields whose strengths are given the above mapping. The simulation results are then transformed back to heavy-ion parameters by the corresponding inverse mapping.

2 Design Features of the Prestripper Linac

Table I shows the basic parameters of the accelerating and focusing lattices of the low-β linac section. It consists of an array of 85 SC cavities distributed in ten cryostat modules. Transverse focussing is provided by SC solenoids contained in the same cryostat modules as the cavities. The lattice in the initial part of the low-β linac consists of a solenoid following each cavity. The final lattice has one solenoid following three cavities. Such arrays, with the cavities operated at a synchronous phase φ = -30°, provide strong focussing in both transverse and longitudinal phase space. Prior to numerical ray-tracing a two-charge-state beam through the low-beta section, the transverse beam motion is matched carefully with the help of fitting codes using a trial beam of single charge state q=28.5. A particularly critical aspect of fitting is to avoid beam mismatch at the transitions between cryostats. Beam dynamics in the SRF linac was simulated using the codes TRACK and 'elegant'. The phase setting for a uranium beam of average charge state q=28.5 is generated by a preprocessor step. The rf phase is set -30° with respect to the maximum energy gain in each SRF cavity.

The beam dynamics simulation included the following steps:

- Beam matching in transverse and longitudinal phase spaces for a trial beam with charge-to-mass ratio of mean value 28.5. The simulation of the trial ion beam was done to minimize beam sizes, and to obtain smooth rms envelopes in the transverse planes. The rms oscillations in longitudinal phase space due to the effect of inter-cavity drift spaces were minimized but not eliminated completely. In the most part of the linac the synchronous phase was set to –30°, which produces a sufficiently linear region for the beam size oscillations. Consequently, the longitudinal emittance of the trial beam does not grow.
- Simulation of two-charge-state beam, leading to final determination of the beam energies at the stripping foil, and the required total number of cavities.
- Beam dynamics simulation of the two-charge-state beam subject to accelerating field phase and amplitude random errors.

Beam mismatch in both transverse and longitudinal phase space is a critical issue at the drift space between the first two cryostats, where the beam energy is low ~700 keV/u. The matching between these two cryostats was accomplished with a specially designed transition section shown in Fig. 1. The last cavity in the cryostat 1 is a 2-gap QWR (type III, see Table I) and was tuned at -40° synchronous phase in order to create time focus at the entrance of the second cryostat. A drift space between the first two cryostat was set to 60 cm, which gives sufficient space to install end covers of the cryostats, vacuum valves, and several units of beam instrumentation.

The cryostat structures containing two types of SRF cavities are shown in Fig. 2. As seen in the figure, the focusing period of the cryostat contains two 57.5 MHz cavities per period, except for the first period ,which forms a focusing period with a "missing" cavity. The space previously allocated to the "missing" cavity was replaced by the inter-cryostat drift. The flange-to-flange distance between the elements located in adjacent cryostats was set to be 40 cm. The focusing structure with "missing" cavity is extremely helpful for transverse beam dynamics tuning. Some adjustment of the focusing fields in the outermost solenoids was required for matching the beam. A similar focusing structure was designed for the cryostats containing the 115 MHz SRF cavities.

Table I. Basic parameters of the low-β linac section.

Beam energy, MeV/u	0.17-0.32	0.32-0.77	0.77-4.35	4.35-9.43
Frequency (MHz)	57.5	57.5	57.5	115
Number of cavities per focusing period	1	1	2	3
Number of cavities	2	5	37	41
Number of cryostats	1		4	5
Type of cavity	4-gap, λ/4 type I	4-gap, λ/4 type II	2-gap, λ/4 type III	2-gap, λ/4 type IV
Geometrical beta, β_G	0.024	0.031	0.061	0.15
Beam steering compensation in the SRF cavity	No	No	No	Yes
Accelerating field (MV/m)	4.0	4.0	5.0	5.0
Synchronous phase (deg)	-30	-30	-30	-25
Random RMS fluctuation of RF field phase (deg)	0.6	0.6	0.3	0.3
Random RMS fluctuation of the field amplitude (%)	0.3	0.3	0.3	0.3
Effective length of solenoids (cm)	10	10	18	30
Type of solenoid	I	I	II	III
Length of focusing period (cm)	54.9	63.3	113.0	177.3
Focusing field (T)	7.0-8.2	8.5-9.1	6.0-11.0	8.2-10.2

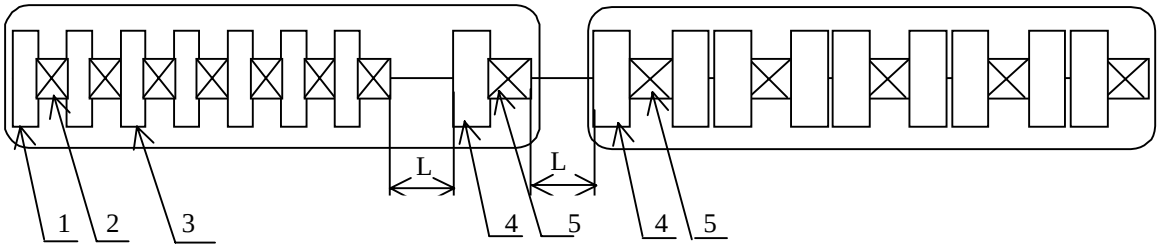

Figure 1. Layout of the first two cryostats of the low-β linac. 1 – Type I SRF cavity, 2 – Type I solenoid, 3 – Type II SRF cavity, 4 – Type III SRF cavity, 5 – Type II solenoid.

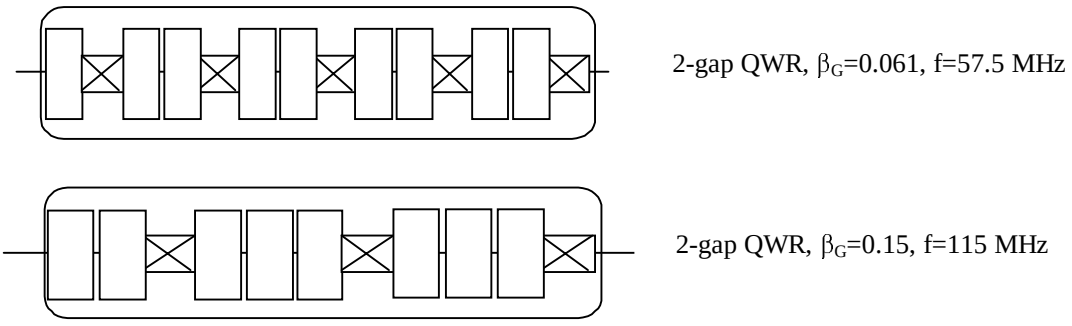

Figure 2. Layout of the cryostats for two different types of cavities.

The rms and total beam envelopes of the two-charge-state beam along the low-β linac are shown in Fig. 3. Due to the perfect transverse matching there is no emittance growth even for two-charge-state uranium beam. The initial phase space distribution used for each charge state was obtained from output distributions at the exit of the RFQ obtained with the DYNAMION code [3]. Fig. 4 shows the longitudinal phase space at the entrance of the SRF linac. The longitudinal effective emittance containing 100% of the uranium beam of charge states 28 and 29 is

2.32 π·keV/u·nsec. In the longitudinal phase space, the two-charge-state beam emittance is always larger than that of a single charge-state beam. Growth in effective emittance occurs due to the oscillations caused by the slightly differing off-tune synchronous phases for the two charge states 28^{+} and 29^{+}. The effective emittance of the two charge-state beam oscillates along the linac as is seen from Fig. 5. There are several obvious causes for these oscillations, among which the distinct synchronous phase for each kind of particle, and mismatched motion due to inter-cryostat spaces. A frequency jump by a factor of two at 29.36 m does not introduce an additional emittance growth due to favourable beam parameters in this transition. Although the effective emittance value can be ~3.5 times larger than the input emittance, the total emittance of the two charge-state beam remains well inside the stable area in longitudinal phase space, as shown in Fig. 4. The beam energy at the exit of the low-β section should be selected so as to obtain the lowest effective emittance for the two-charge-state beam. This feature is a very important factor in maintaining low emittance along the whole driver linac.

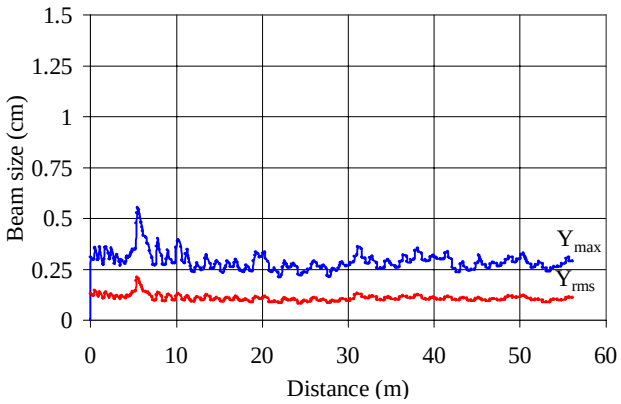

Figure 3. Two charge-state beam rms and maximum sizes in vertical plane along the low-β linac. The red curve indicates the rms beam envelope, the blue curve indicates the beam maximum envelope.

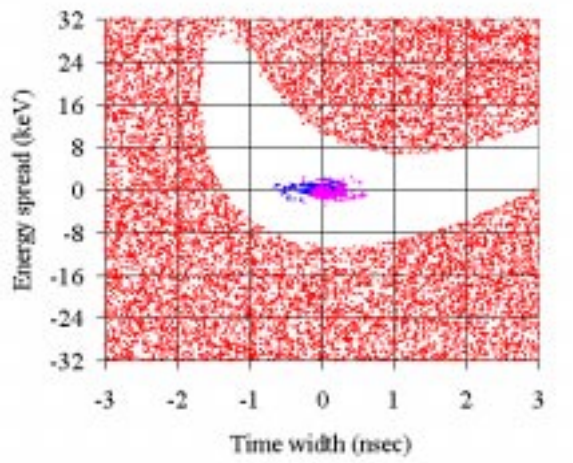

Figure 4. Longitudinal acceptance of the low-β SRF linac. The blue and magenta dots show the longitudinal phase space plots of uranium beam with charge q=28+ and q=29+ obtained at the RFQ exit.

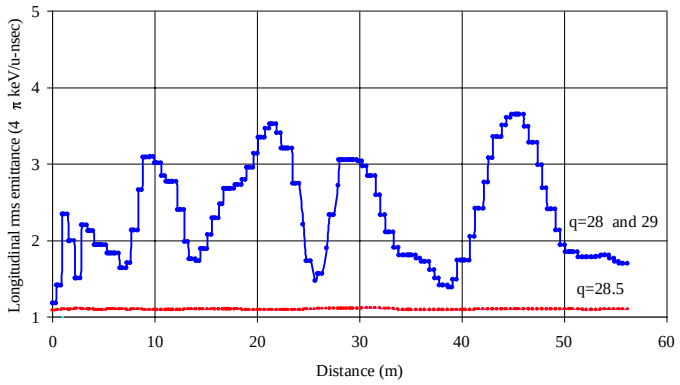

Figure 5. RMS longitudinal emittance variation of single- and two charge-state beams along the low-β linac.

3 Effects of Combined Errors on Longitudinal Beam Parameters

All errors were randomly generated as a uniform distribution with rms values δ_i listed in Table I. Accordingly the interval of error distribution is $\pm\sqrt{3}\cdot\delta_i$. Sensitivity of the multi-charge beam parameters to various types of random errors were studied. Phase and amplitude errors of the rf field are fast fluctuations and produce effective emittance growth of the two-charge state beam. Simulations of the beam dynamics under these errors were performed at the magnitudes listed in Table I , and their effect on the longitudinal effective emittance of the two-charge-state beam was determined. The error magnitudes were based on the ATLAS accelerator performance. Table II summarizes the combined-errors effect on the longitudinal emittance of the two-charge-state beam in the low-β section. Phase space plots obtained for 200 seeds were accumulated and are shown in Fig. 6. As seen in the figure, the emittance of the two charge-state beam remains much smaller than the acceptance of the following linac section.

Table II. Summary of longitudinal beam emittance at the exit of low-β section.

Parameter	Emittance π·keV/u·nsec
4RMS emittance of single charge-state beam	1.2
4RMS emittance of two charge-state beam	1.7
4RMS emittance of two charge-state beam with errors	1.9
98% emittance of two charge state beam accumulated during 200 random seeds	3.9
100% emittance of two charge state beam accumulated during 200 random seeds	10.0

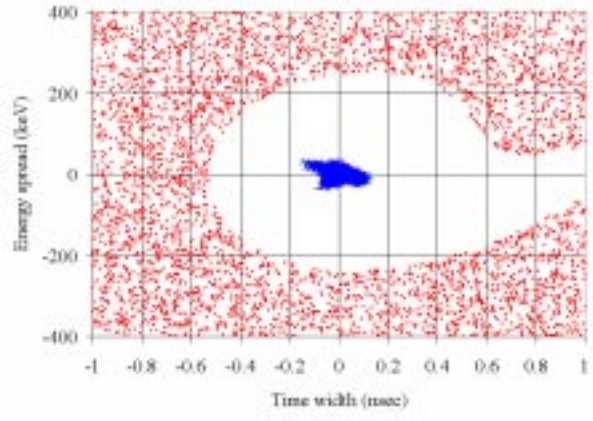

Figure 6. Longitudinal acceptance of the medium-β SRF. The blue dots represent the longitudinal phase space of the uranium beam with charges q=28+ and q=29+ ,accumulated for 200 simulations under combined random phase and amplitude fluctuations of the accelerating field.

4 Effects of Single Errors on the Longitudinal Emittance

Random rf phase errors and field strength errors for the two-charge state 28^+ and 29^+ of Uranium beam were simulated using the program 'elegant'. Each error type was simulated at three error levels and for 200 distinct seeds. We considered phase errors of 0.3, 0.6 , and 0.9 deg. Electromagnetic field strength errors varied from 0.3, to 0.6, and 0.9 %. Table III shows the effects of these individual errors on the longitudinal 4rms emittance at the end of the prestripper linac. In the table, the second and third columns represent the 200 seeds-distribution average and rms values of the 4rms emittance, respectively. The emittance values resulting from phase fluctuations and field strength fluctuations at equivalent levels are comparable, as expected for the error amplitudes analysed, since the phase-space area deviation can be written as:

$$\delta A = \delta E / E + \delta \Phi \tan \Phi,$$

where E is the accelerating field and Φ is the rf-phase.

Fig. 7 (a) and (b) show the emittance variation with phase fluctuations and field strength fluctuations, respectively.

Table III. 4rms Emittance at the End of the Prestripper Linac Under Single Random Errors.

Phase Error (degrees)	4RMS Emittance (π keV/u-ns) Calculated Average over 200 Seeds	4RMS Emittance (π keV/u-ns) Calculated RMS over 200 Seeds
0.3	2.17	2.23
	2.36	2.51
0.9	2.70	2.93
Field Strength Error (%)		
0.3	2.18	2.22
0.6	2.34	2.47
0.9	2.66	2.87

In the plots, ε_{98} represents the total phase space area calculated as the superposition of the phase space distributions at the exit of the low β section, from which the distributions resulting in the four highest emittances were eliminated. The emittance grows exponentially with the error magnitude, as expected for random distributions, and at similar rates for both types of errors, as aforementioned. The ε_{98} emittance, resulting from phase or field errors at the largest level, is of the order of 9 keV/u-nsec, a factor of 2.5 times the ideal total emittance of 3.4 keV/u–ns, corresponding to 2 times the two-charge-state 4RMS emittance given in Table II.

Fig. 8-(a) shows a typical histogram of the 200-sample distribution for field strength errors at 0.9 % rms. The emittance growth, defined as the ratio of the emittances at the entrance and exit of the prestripper linac, is histogrammed against the percentage of simulations resulting in the corresponding emittance growth value. In the figure, the distribution rms and mean values are also shown. The histogram follows a Poisson distribution, indicating the independent nature of each result. Figure 8 (b) depicts the corresponding probability distribution function (PDF) of the emittance growth factor. As can be seen in the figure, there is 98% probability that the emittance growth factor be less than 6.4. The larger PDF values are the contributions from the four rightmost outliers seen in Fig. 8(a).

The accumulated 200 phase space distributions at the end of the prestripper linac resulting from phase errors at 0.3° and field strength errors at 0.3% are plotted in Fig. 9-(a) and 8-(b), respectively. The corresponding phase–space distributions from errors at the levels of 0.9 deg and 0.9% are shown in Fig. 8-(c) and 8-(d), for comparison. No particles are lost, and the final distributions are well within the longitudinal acceptance of the low-β SRF linac.

Effects of construction errors and misalignments on the two-charge state beam dynamics and correction methods are now being studied. The analysis includes 6D electromagnetic field and 3D solenoid field distributions. The results will be used to establish a detailed tolerance budget for the prestripper SRF linac.

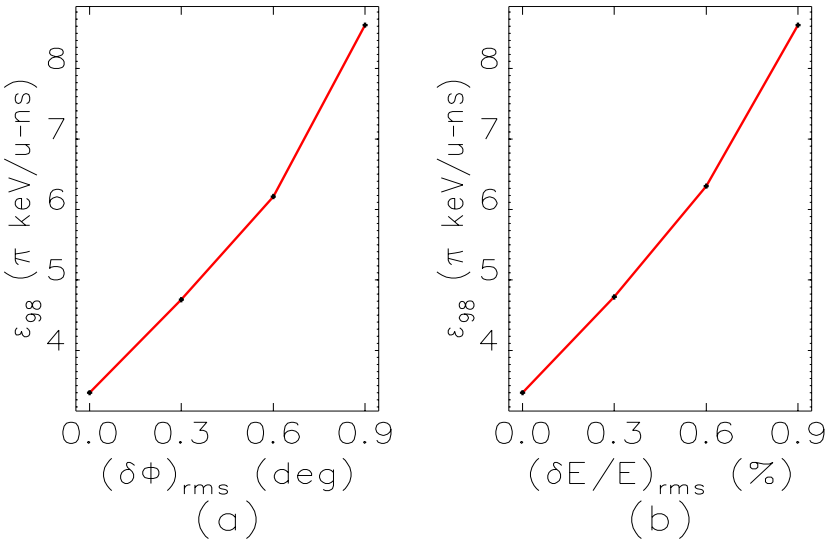

Figure 7: Accumulated longitudinal emittance versus rf phase fluctuations (a) and accelerating field strength fluctuations (b). ε_{98} represents the superposition of the phase space areas at the exit of the prestripper linac, from which the distributions with the four largest areas were eliminated.

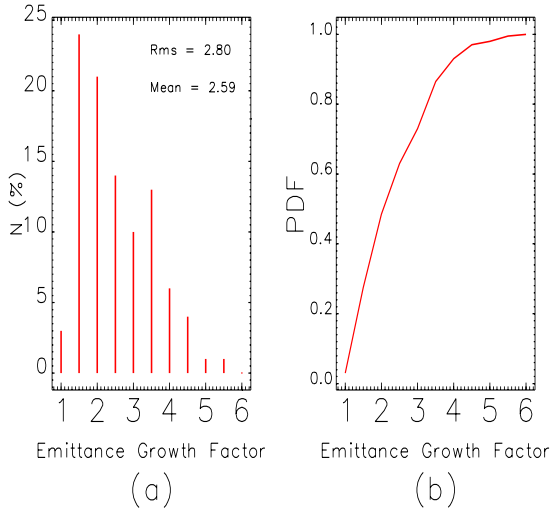

Figure 8: Histogram (a) over 200 simulations of the emittance growth factor, defined as the ratio of the initial and final emittances for the 200 simulations, and the corresponding probability function (b). The frequencies are expressed in terms of the percentages of simulations resulting in the emittance values indicated.

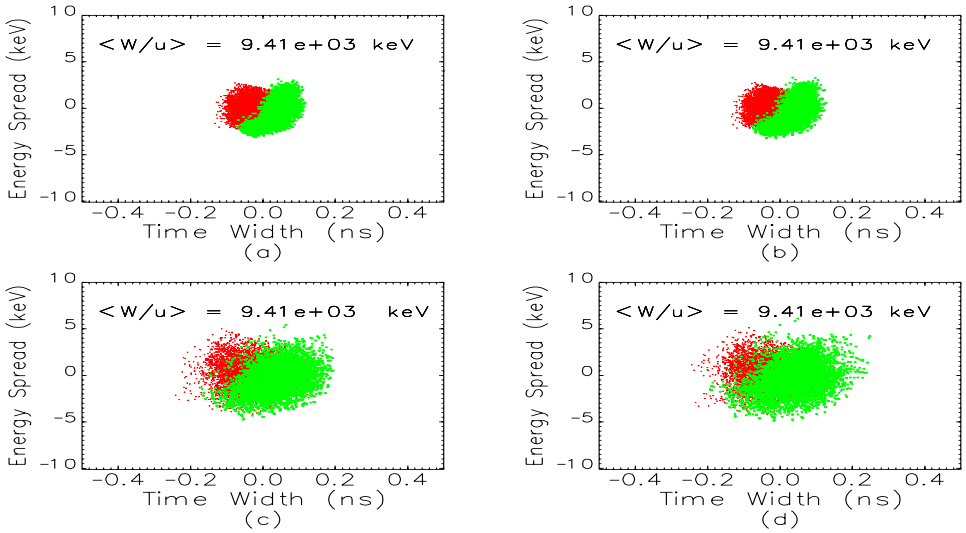

Figure 9: Accumulated longitudinal phase space distribution at the exit of the low β linac, resulting from phase errors of 0.3 ° (a), and from field strength errors of 0.9% rms (b). (c) and (d) depict the distributions from 0.9 ° phase and 0.9% strength errors, respectively. The red dots represent q=29 particles, and the blue dots represent q=28 particles.

References

1. P.N. Ostroumov, et al., Heavy-Ion Linac Development for the U.S. RIA Project. In this Proceedings.
2. P. N. Ostroumov and K. W. Shepard, Multiple-Charge Beam Dynamics in an Ion Linac, Phys. Rev. ST Accel. Beams **3**, 030101 (2000).
3. P.N. Ostroumov et al, "Heavy Ion Beam Acceleration of Two Charge States from an ECR Ion Source" in Proceedings of the XX International Linac Conference, Monterey, California, August 21-25. SLAC-R-561, v.1, p. 202.
4. P. N. Ostroumov and K. W. Shepard, Correction of Beam Steering Effects in Low-Velocity Superconducting Quarter-Wave Cavities, Phys. Rev. ST. Accel. Beams **11**, 030101 (2001).
5. CST Microwave Studio, User Manual Version 3.0, January 2001, CST GmbH, Darmstadt, Germany.
6. M. Borland, "elegant: A Flexible SDDS-Compliant Code for Accelerator Simulation," APS-LS-287, http://www.aps.anl.gov/techpub/lsnotes/ls287.pdf.
7. M. Borland and L. Emery, "The Self-Describing Data Set Files Protocol and Toolkit," Proc. 1995 ICALEPS Conference, October 1995,Chicago.